8

Atom Manipulation on Semiconductor Surfaces

Yoshiaki Sugimoto

Abstract. Since the sophisticated atom manipulation experiment reported by Eigler, single atom manipulation and assembly by scanning tunneling microscopy (STM) has attracted much attention because of the intriguing applications in nanofabrication and nanoscience. In recent years, we have developed an atom manipulation technique using atomic force microscopy (AFM), which has proven to be a powerful tool for imaging individual atoms on insulating as well as conducting surfaces, force spectroscopic measurements between single atoms, and even chemical identification. After the first demonstration of the vertical and lateral manipulation of single atoms using AFM at low temperature, we have achieved well-controlled atom manipulation and assembly on semiconductor surfaces even at room temperature. The new method to enable us to rearrange surface adatoms at room temperature is based on an interchange of different atom species.

8.1 Introduction

The ability to engineer nanostructures with unique and specific properties is a key technology for developing the next generation of novel nanoelectronic devices. For this tremendous goal, major success is anticipated through the bottom-up approach: an attempt to create such nanodevices from the atomic or molecular level instead of miniaturizing from the macroscopic world. In the bottom-up approach, the ultimate limit is to engineer artificial nanostructures on surfaces by manipulating single atoms or molecules one by one. In 1990, Eigler reported that single atoms can be laterally manipulated on a surface to create an artificial nanostructure using a scanning tunneling microscope (STM) [1]. Since then, only a few groups worldwide have developed the required STM technology for nanostructuring on a surface by precisely allocating single atoms and molecules at desired positions [2,3]. The technique has developed to a point that it is possible to build a logic gate [4] based on a few hundred molecules, or to complete the initial stage of wiring a single molecule and to study the electrical properties of this metal–molecule–metal junction [5]. Most of these technologically promising experiments [1–14], however,

S. Morita et al. (eds.), *Noncontact Atomic Force Microscopy*,
NanoScience and Technology,
DOI: 10.1007/978-3-642-01495-6_8, © Springer-Verlag Berlin Heidelberg 2009

must be performed at low temperature (LT), where the low thermal energy of the atoms at the surface guarantees the stability of the artificially created nanostructure, avoiding diffusion or desorption. To achieve nanodevices operative in ambient conditions, strategies for atom-by-atom construction of stable nanostructures at room temperature (RT) are highly desirable.

STM was the only tool with all the necessary capabilities for manipulating single atoms and molecules and arranging them on a surface at will until true atomic resolution using an atomic force microscope (AFM) was achieved [15–17]. Our group has developed an atom manipulation technique using AFM and it was demonstrated that AFM can manipulate atoms, even at RT, with high precision, comparable to previous STM studies [18, 19].

In this chapter, we review atom manipulation experiments on semiconducting surfaces that our group has performed during the past several years. The first experimental evidence of reproducible mechanical vertical manipulation of selected single atoms of a surface using AFM was reported in 2003 [20]. In vertical atom manipulation, atoms are vertically transferred between tip and surface. Atom extraction from a surface is illustrated in Fig. 8.1a. In 2005, lateral manipulation of single atoms that adsorbed on a surface at LT was reported [21]. In lateral atom manipulation, single atoms that always stay on the surface are laterally manipulated as shown in Fig. 8.1b. Then atom

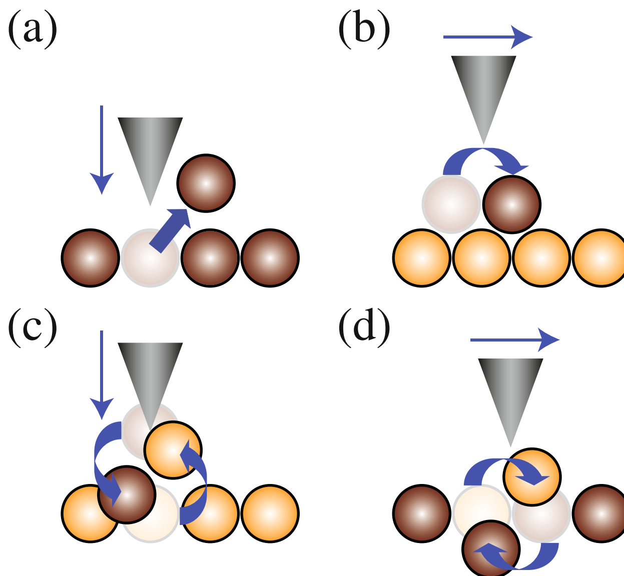

Fig. 8.1. Classification of atom manipulation modes demonstrated by AFM. (**a**) Vertical atom manipulation, (**b**) lateral atom manipulation, (**c**) interchange vertical atom manipulation, and (**d**) interchange lateral atom manipulation. The latter two methods enable us to manipulate single atoms at room temperature

manipulation and assembly at RT with similar precision to that obtained in LT manipulation experiments using STM was demonstrated [18]. This RT technique is based on a novel method that we call interchange lateral atom manipulation, in which two different atomic species are interchanged in the plane of a heterogeneous surface, as shown in Fig. 8.1d. In 2007, a combination of conventional lateral atom manipulation experiments and first-principle calculation clarified the mechanism of mechanical lateral atom manipulation on the Si(111)-(7×7) surface at RT [22]. Moreover, in 2008, we demonstrated a novel method for engineering nanostructures on surfaces at RT by vertically interchanging tip apex atoms and single surface atoms as shown in Fig. 8.1c [19], a technique we call interchange vertical atom manipulation.

The remainder of this chapter is organized as follows. First, the experimental method is described in Sect. 8.2. Second, we present vertical atom manipulation in Sect. 8.3, lateral atom manipulation at LT in Sect. 8.4, interchange lateral atom manipulation in Sect. 8.5, lateral atom manipulation at RT in Sect. 8.6, and interchange vertical atom manipulation in Sect. 8.7. Finally, concluding remarks are presented in Sect. 8.8.

8.2 Experimental

We have used two similar types of ultrahigh vacuum AFM, of which one works at RT and the other at LT [23]. The deflection of commercial Si cantilevers with a typical spring constant of $30\,\mathrm{N\,m^{-1}}$ and first resonant frequency of 160 kHz (NanoWorld AG, Neuchatel, Switzerland) was detected using a home-built interferometer. A sharp, clean Si tip apex was prepared by Ar ion sputtering in ultrahigh vacuum. The cantilever dynamics were detected and regulated using phase-locked loop-based commercial electronics (Nanosurf AG, Liestal, Switzerland). A constant amplitude mode was applied for cantilever oscillation, except for the vertical atom manipulation experiments in Sect. 8.3, where a constant excitation mode was used. The cantilevers were oscillated at relatively large amplitudes (on the order of 10 nm) to maintain a stable oscillation amplitude [24]. The shift in the cantilever's first mechanical resonant frequency (frequency shift, Δf) was the observable used for controlling the tip–surface distance. Data acquisition, microscope operation, force spectroscopy, and single atom manipulation processes were performed through a very versatile commercial scanning probe controller based on digital signal processor technology (Nanotec Electronica S.L., Madrid, Spain) [25].

We used two substrates of Si(111) and Ge(111) for atom manipulation experiments. A clean Si(111)-(7×7) surface was obtained from an n-type single crystal Si wafer by direct current heating, flashing the sample up to 1,200°C with subsequent slow cooling from 900°C to RT. During sample preparation, vacuum pressure was kept below 1×10^{-10} Torr. This surface was used for vertical atom manipulation in Sect. 8.3 and lateral atom manipulation at RT in Sect. 8.6. Sn/Si(111)-($\sqrt{3} \times \sqrt{3}$), In/Si(111)-($\sqrt{3} \times \sqrt{3}$), and

Sb/Si(111)-(7 × 7) surfaces were used for the interchange lateral atom manipulation described in Sect. 8.5. These surfaces were prepared by evaporating Sn, In, or Sb atoms on the Si(111)-(7 × 7) surface followed by annealing the sample [26, 27]. The Sn/Si(111)-($\sqrt{3} \times \sqrt{3}$) surface was also used for interchange vertical atom manipulation, as described in Sect. 8.7.

Clean reconstructed Ge(111)-c(2 × 8) surfaces were prepared by successive cycles of Ar ion sputtering while heating the sample at 500°C. Typical ion bombardment parameters were 1 keV of ion beam energy, with an ion current measured at the sample of approximately 4 μA and a 45° of incidence angle. After the ion bombardment, upon recovering a vacuum pressure of less than 1×10^{-10} Torr, a further sample annealing at 750°C for 3 min followed by a slow cool-down to RT completed the surface preparation. Ge(111)-c(2 × 8) surfaces were used for lateral atom manipulation at LT in Sect. 8.4. Sn/Ge(111)-c(2 × 8) surfaces were prepared for interchange lateral atom manipulation in Sect. 8.5. This surface was prepared by evaporating a small number of Sn atoms on the Ge(111)-c(2 × 8) surface and then annealing the surface [28].

8.3 Vertical Atom Manipulation

First, we present the first experimental evidence, to our knowledge, of the reproducible mechanical vertical manipulation of selected single atoms of a surface by using AFM [20]. The method is based on a carefully controlled soft nanoindentation process at a constant excitation mode of the cantilever oscillation using LT-AFM (80 K). The results of vertical manipulation of Si adatoms on the Si(111)-(7 × 7) surface are shown in Fig. 8.2. After taking an atomically resolved image over a region centered on one terrace of the surface [Fig. 8.2a], a specific Si adatom in the imaged area was selected for manipulation, as shown by the circle. The tip was positioned directly above this target Si adatom, and the tip–sample distance was gradually decreased from the imaging distance by applying a ramp voltage to the electrode of the piezo-electric scanner with the feedback loop open. Since the cantilever was oscillating at its first resonant frequency, multiple nanoindentation processes took place during the sample approach. The nanoindentation process was carefully controlled by simultaneously monitoring both the variations of the cantilever oscillation amplitude and Δf. Upon further indentation, a sudden jump in Δf was normally detected. At this point, the ramp was stopped, the tip–sample distance was increased to the initial distance, and the feedback was reactivated. Figure 8.2b is the image obtained with the same parameters used for taking the initial image. The selected Si center adatom marked with a circle in Fig. 8.2a was removed from its initial position, and a vacancy was created without additional perturbation of the Si(111)-(7 × 7) unit cell. This fact implies that at least three strong covalent bonds that fixed the Si adatom to the surface were broken during nanoindentation. Moreover, the deposition of a single atom can be performed over the created vacancy in Fig. 8.2b by the

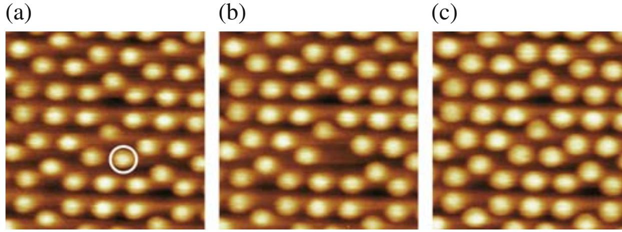

Fig. 8.2. Sequence of AFM topographic images showing mechanical vertical atom manipulation. A single Si adatom marked with a circle in (**a**) was removed by vertical approach of the tip toward the Si adatom. A single atom was deposited on the created vacancy site visible in (**b**). As a result, the perfect surface was restored as shown in (**c**). Image size is $47 \times 47\,\text{Å}^2$. The cantilever oscillation amplitude (A) and Δf were 257 Å and -4 Hz, respectively [20]

same method as that applied for atom extraction. Figure 8.2c shows that a single atom transferred from the tip restored the initial unperturbed structure of the Si(111)-(7×7) half-cell. This result implies the possible formation of three new covalent bonds, as the deposited atom adapted to a central adatom position of the Si(111)-(7×7) reconstruction.

This experiment proved that AFM has enough precision to perform vertical manipulation of single atoms. Soon after, it was demonstrated that the same technique can be used for vertical atom manipulations on the same surface even at RT [29].

Previous STM studies on manipulation of the bare Si(111)-(7×7) surface suggested that the mechanism for removing single Si adatoms at RT was thermally activated field ion emission due to a high electric field between tip and sample during the application of a voltage pulse [14,30,31]. This could also be the mechanism for the modification of the Si(111)-(7×7) surface performed at LT using AFM by applying a voltage pulse between tip and sample [32]. An alternative mechanism was proposed for the lateral displacement of single Si adatoms on the same surface performed by LT-STM, where tunneling electrons from the STM tip, temporally occupying a surface resonance state, could play a fundamental role [33]. Nevertheless, a completely different mechanism for manipulating Si adatoms should be involved in the mechanical atom manipulation presented here, because neither a bias voltage nor a voltage pulse was applied between the AFM tip and the sample during the manipulation process. See Chap. 11 for the detailed mechanism of mechanical vertical atom manipulation.

8.4 Lateral Atom Manipulation at Low Temperature

The first lateral atom manipulation using AFM has been demonstrated using the same LT apparatus as that used for the first vertical atom manipulation experiment in Sect. 8.3. An adsorbate deposited from the tip on a clean

Ge(111)-c(2×8) surface was laterally manipulated at 80 K [21]. The adsorbate was imaged as a bright spot in AFM images, as shown in Fig. 8.3a. Individual Ge adatoms on the Ge(111)-c(2×8) substrate were also observed with slight contrast. Scanning at a far enough tip-surface distance, characterized by a Δf set point for imaging ($\Delta f_{\mathrm{image}}$), it can be seen that this adsorbate remained unperturbed at the surface during imaging (Fig. 8.3a). In contrast, two bright spots instead of one were observed in a subsequent image (Fig. 8.3 b). In this image, the tip was scanned from the bottom to the horizontal dotted line with slightly reduced tip–surface distance by changing the set point to the value for manipulation (Δf_{move}). Then from the horizontal dotted line to the top, the tip–surface distance was increased by restoring the $\Delta f_{\mathrm{image}}$ set point. A possible explanation of the double protrusions observed in Fig. 8.3b is that after the adsorbate at the initial position was imaged, it jumped to the next stable adsorption position in the same direction as the slow scan, and then the same adsorbate was imaged again. No additional atom movement was observed after recovery of the tip–surface distance.

In the same way, the adsorbate was consecutively manipulated along the $[1\bar{1}0]$ direction as shown in Figs. 8.3 (c)–(h). The arrows indicate the slow scan direction; the solid (dotted) arrows correspond to imaging at Δf_{move} ($\Delta f_{\mathrm{image}}$), respectively. Dotted lines indicate the slow scan position at which the set point was switched from Δf_{move} to $\Delta f_{\mathrm{image}}$. As Fig. 8.3b–h illustrates, the adsorbate was manipulated as following the slow tip scan when imaging at high attractive interaction force (Δf_{move}), and it stopped near the line at which the interaction force was released. While in Fig. 8.3b–d, f, and g, the adsorbate was manipulated to the next stable adsorption position, in Fig. 8.3e, h, the atom was manipulated along the $[1\bar{1}0]$ direction repeatedly until the tip–surface distance was increased. Additionally, while in Fig. 8.3b–e, g, the adsorbate was displaced upwards, in Fig. 8.3f, h, it was manipulated downward according to the set slow scan direction. Finally, in Fig. 8.3h, the adsorbate was manipulated until it was almost returned to the surface position where it was initially deposited (Fig. 8.3a). These experimental results showed that this atom hopping can be controlled by tuning the distance between the sample and the oscillating AFM tip.

The lateral atom manipulations shown in Fig. 8.3 were performed by forward and backward fast line scans parallel to the $[11\bar{2}]$ crystallographic direction. In tip-induced movement of an adsorbate placed in a homogeneously distributed surface potential, one should expect lateral displacements along the fast line scan direction too. These lateral displacements were, however, not observed (Fig. 8.3); thus, the adsorbate movement should be confined along the adatom rows by greater diffusion energy barriers in the $[11\bar{2}]$ crystallographic direction than in the $[1\bar{1}0]$ one.

This manipulation process can be categorized as the pulling mode proposed in previous lateral atom manipulation using LT-STM [34], because this jump occurs after imaging the adatom as it followed the slow tip scan. The experiment demonstrated in Fig. 8.3 is the first clear evidence of the AFM

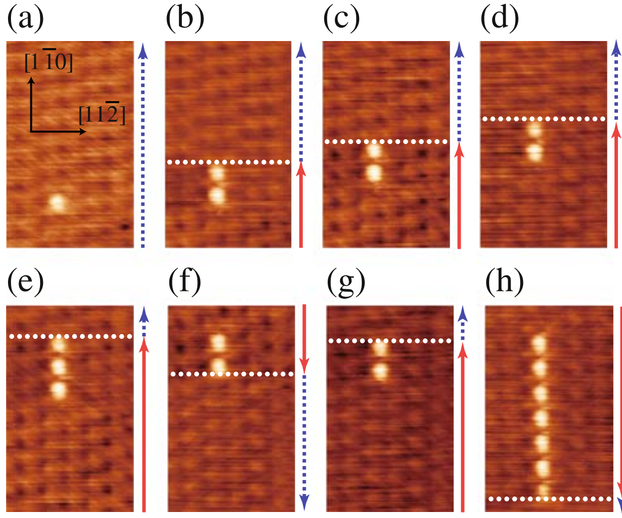

Fig. 8.3. (**a**)–(**h**) Sequence of consecutive topographic AFM images showing the lateral manipulation of an adsorbate deposited on top of a Ge(111)-c(2×8) surface. This adsorbate is manipulated by changing the slow scan direction and the tip–surface distance as indicated by the arrows beside each image. Scanning at a close tip–surface distance (*solid arrows*) corresponds to $\Delta f_{\mathrm{move}} = -32.0\,\mathrm{Hz}$. Scanning at a distance at which the adatom remains unperturbed (*dotted arrows*) corresponds to $\Delta f_{\mathrm{image}} = -28.8\,\mathrm{Hz}$. The scan line at which the change between these two Δf values was made is indicated by a *dotted line* in each image. The image size is $2.2 \times 3.5\,\mathrm{nm}^2$. The spring constant ($k$), the first mechanical resonance frequency (f_0), and A are $33.2\,\mathrm{N\,m}^{-1}$, 167,485.8 Hz, and 9.3 nm, respectively. The temperature of the tip and sample was kept at 80 K [21]

capability for laterally manipulating adsorbates deposited on top of a surface, and it opened up new and very exciting perspectives for this technique.

8.5 Interchange Lateral Atom Manipulation

After the first demonstration of the vertical and lateral manipulation of single atoms using AFM at LT as described earlier, we discovered a new method that enables us to manipulate single atoms even at RT. As a result, we have achieved well-controlled atom manipulation and assembly on the Sn/Ge(111)-c(2×8) surface at RT [18]. In this method, which we call interchange lateral atom manipulation, substitutional Sn adatoms in the plane of the Ge surface can be individually manipulated by a tip-induced interchange with the surrounding surface Ge adatoms. This novel atom manipulation can be controlled by an appropriate selection of the tip scan direction, and by tuning the attractive interaction force acting between tip and surface.

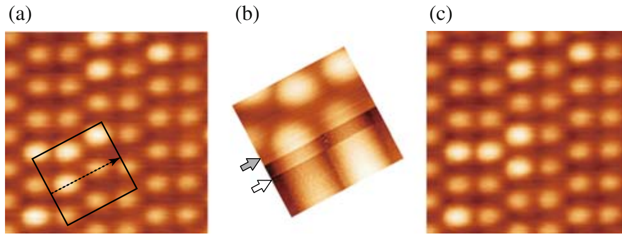

Fig. 8.4. Sequence of AFM topographic images showing the method for interchange lateral manipulation of substitutional Sn adatoms on the Ge(111)-c(2×8) surface. (**a**) After imaging the surface at tip–surface interaction forces that do not activate the interchange between Sn and Ge adatoms, the scan size was reduced and the tip fast-scan direction was aligned with the line connecting the centers of the adatoms selected for manipulation, as indicated by the square and the dotted arrow, respectively. (**b**) The surface was imaged until the slow scan reached the line connecting the centers of the adatoms (marked with a *gray arrow*), and the slow scan was stopped at this line. Successive topographic scans over this line with gradually reduced tip–surface distance led to the adatom interchange. This process is monitored by a swap in the height signals associated with each adatom type (see the *white arrow*). These line-scans were performed by lifting the oscillating tip, typically 1 Å above the surface, on the way back. (**c**) The surface area was imaged again without perturbing the adatoms. Image size is $4.6 \times 4.6\,\mathrm{nm}^2$ for (**a**) and (**c**), and $1.9 \times 1.9\,\mathrm{nm}^2$ for (**b**). AFM acquisition parameters were $A = 176$ Å with a cantilever of $k = 34.8\,\mathrm{N\,m}^{-1}$ and $f_0 = 169.430$ kHz. Δf value is -8.3 Hz for (**a**) and (**c**), and -11.3 Hz in (**b**) [18]

Figures 8.4 show the procedure for manipulating a substitutional Sn adatom on the Ge(111)-c(2×8) surface. First, we obtain an AFM topographic image of the Sn/Ge(111)-c(2×8) surface, as shown in Fig. 8.4a. In this initial image, where Sn adatoms appear slightly brighter than Ge adatoms, an Sn adatom and a first neighboring Ge adatom are chosen for manipulation. Next, a small area is scanned by rotating the scan angle, as indicated by the square in Fig. 8.4a. The scan direction is selected such that the fast scan direction is aligned with the vector that connects the positions of the selected Sn and Ge adatoms. The fast scan begins near the position occupied by the Sn adatom, and ends near the Ge adatom position. At this time, the tip is lifted, typically 1 Å above the surface, on the way back before subsequent scans in the fast scan direction. The result of this scan is shown in the upper half of the image in Fig. 8.4b. The slow tip-scan is stopped when the tip reaches the line connecting the centers of the two adatoms (the gray arrow). The tip successively scans the same line above the arrow in Fig. 8.4a. Then the attractive interaction force acting between the outermost atoms of the tip and the atoms at the surface is gradually increased by reducing the tip–surface distance. At a certain closest approach distance, the attractive interaction force overcomes the threshold value needed for activating the interchange between Sn and Ge adatoms during the line-scan, making the Sn adatom follow the

tip. Successful manipulation can be confirmed by checking the height signals associated with each adatom type, which change in location after the adatom interchange as shown by the white arrow in Fig. 8.4b, in subsequent line-scans. Finally, reducing the attractive interaction force to values at which the adatoms remain unperturbed at their adsorption positions, the surface is imaged again (Fig. 8.4c). By comparing Fig. 8.4a, c, one can confirm that the target Sn adatom is manipulated. The tip–surface interaction force involved in this manipulation is associated with the onset of covalent bond formation between the outermost atom of the tip and the adatoms at the surface, as expected for AFM image formation on a semiconductor surface [17].

To demonstrate the reproducibility of the new lateral manipulation method found at RT, we created an artificial nanostructure atom-by-atom. Figures 8.5 display a selection of sequential AFM images acquired while constructing an "atom inlay," which is an in-plane nanostructure composed of several embedded atoms on a surface. The white arrow in each image indicates the same Sn adatom. By consecutively rearranging substitutional Sn adatoms on the Ge surface, the letters "Sn," the atomic symbol of the element tin, were constructed at RT (Fig. 8.5i). The creation of these nanostructures required more than 120 interchange lateral atom manipulations with continuous AFM operation for 9 h. This new lateral manipulation method is proven to be well controlled even at RT.

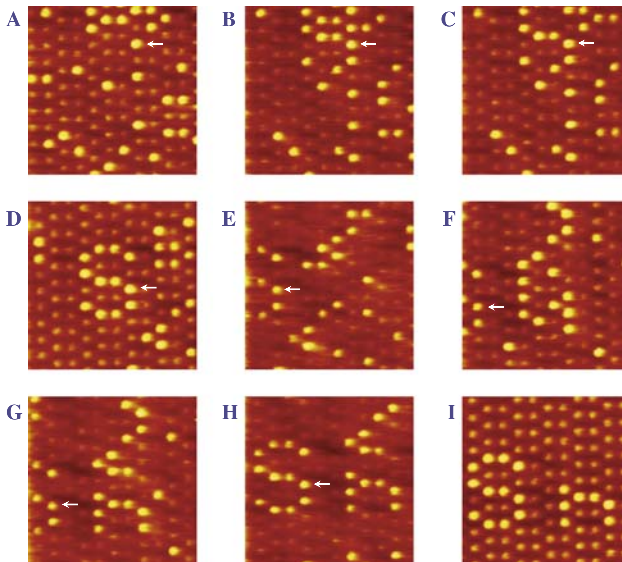

Fig. 8.5. Sequence of AFM images of the process of rearranging single atoms for the construction of an "atom inlay" at RT. Image size is $7.7 \times 7.7\,\mathrm{nm}^2$. The image was acquired with $A = 157\,\text{Å}$, using a Si cantilever of $k = 29.5\,\mathrm{N\,m^{-1}}$, setting a Δf value of $-4.6\,\mathrm{Hz}$ with respect to $f_0 = 160.450\,\mathrm{kHz}$ [18]

Although an atomistic picture of this manipulation mechanism has not been clarified yet, phenomenologically, atom interchange can be attributed to the diffusion process by a tip-induced reduction of the energy barrier. It was reported that substitutional Pb adatoms on the Pb/Ge(111)-c(2×8) surface, which is similar to the Sn/Ge(111)-c(2×8) surface, diffuse by interchanging the positions of Pb and Ge adatoms even at RT [35, 36]. In contrast, the energy barrier for diffusion of substitutional Sn adatoms on the Ge(111)-c(2×8) surface is higher than that for Pb/Ge(111)-c(2×8). We measured the diffusion rate of the substitutional Sn adatoms at RT by continuously imaging the same surface area for more than 6 h with a weak enough tip–surface attractive interaction force [18]. We found that the diffusion rate is less than 5.7×10^{-7} jumps per s per atom. The lower limit of the energy barrier value is determined to be 1.1 eV, which is higher than 0.54 eV, the measured activation energy value for the Pb/Ge(111)-c(2×8) system [36]. We suggest that bonds between Sn adatoms and the first layer of Ge atoms are stronger than those between Pb adatoms and Ge atoms. Nevertheless, the chemical bonding force between the AFM tip apex atoms and the surface adatoms can reduce the energy barrier associated with the Sn-Ge interchange. Additionally, the tip-induced reduction in this energy barrier is very localized, because when the fast tip-scan is properly aligned with the vector connecting the centers of the two adatoms, almost no interchange events with other first neighboring Ge adatoms out of this direction have been detected.

From the diffusion measurements of the Sn adatoms, we can estimate the minimum mean lifetime of the artificial nanostructures shown in Fig. 8.5i. Let us consider that the nanostructure is destroyed when one of the adatoms that compose it thermally diffuses and changes its position. Assuming that this change in position is a statistically independent process, the minimum mean lifetime of the artificial nanostructure would be the minimum mean lifetime of an unperturbed substitutional Sn adatom placed in a well-reconstructed area of the Ge(111)-c(2×8) surface times the number of atoms that compose the nanostructure. Taking into account that the minimum mean lifetime of an unperturbed substitutional Sn is the inverse of the upper limit for the diffusion rate, that is, 1.75×10^6 s, in principle, artificial nanostructures formed in this way could remain stable on the surface at RT for relatively long periods of time. For the nanostructures reported here, a minimum mean lifetime of 25 h is estimated.

In addition, we confirmed that interchange lateral atom manipulation can be applied not only to Sn/Ge(111)-c(2×8) surfaces but also to other alloy systems, such as Sn/Si, In/Si, and Sb/Si systems, even on different surface structures [19, 37]. Sn, In, and Sb atoms are group IV, III, and V elements in the periodic table, respectively. Figure 8.6 shows the results of manipulation on the Sn/Si(111)-($\sqrt{3} \times \sqrt{3}$), In/Si(111)-($\sqrt{3} \times \sqrt{3}$), and Sb/Si(111)-(7×7) surfaces. The upper images (Fig. 8.6a–c) are the AFM topographies before manipulation, and the lower images (Fig. 8.6d–f) are those after manipulation. Two different atomic species marked by dotted rectangles were interchanged

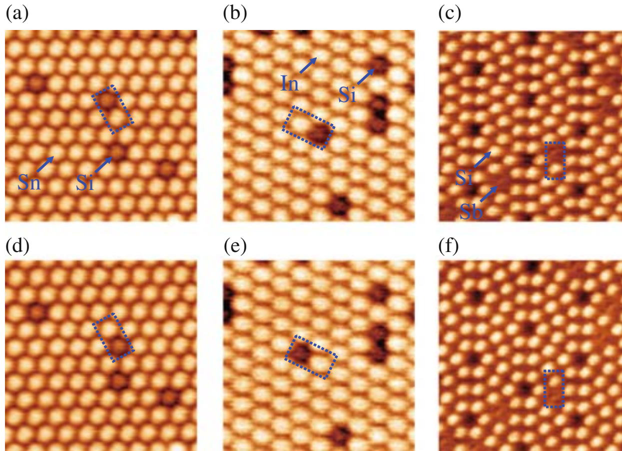

Fig. 8.6. AFM images demonstrating interchange lateral atom manipulation on the various surfaces. (**a**), (**d**) Sn/Si(111)-($\sqrt{3}\times\sqrt{3}$) surface, (**b**), (**e**) In/Si(111)-($\sqrt{3}\times\sqrt{3}$) surface, and (**c**), (**f**) Sb/Si(111)-(7×7) surface. (**a**–**c**) are before manipulations and (**d**–**f**) are after manipulations [19, 37]

by the method described above. Note that while the Sn/Ge(111)-c(2×8) and Sb/Si(111)-(7×7) surfaces have restatoms, Sn/Si(111)-($\sqrt{3}\times\sqrt{3}$) and In/Si(111)-($\sqrt{3}\times\sqrt{3}$) do not: all dangling bonds of the first-layer Si atoms are saturated. Thus, this result clarifies that restatoms are not requisite for the atomic interchange process. The experimental results imply that the in-plane atomic interchange process is based on a common mechanism independent of the surface structure and elements.

The experiments described here show the capability of AFM for engineering nanostructures by rearranging surface adatoms on various semiconductor surfaces at RT. Since nanostructures incorporated into the surface remain stable for relatively long periods of time even at RT, the study presented here paves the way for various applications, such as the construction of artificial nanodevices and dopant arrangement in semiconductor surfaces with atomic precision.

8.6 Lateral Atom Manipulation at Room Temperature

Despite the success of AFM manipulation at RT, resulting from the discovery of interchange lateral atom manipulation, the atomistic mechanism of this new method remained unclear. To shed some light on the mechanism of RT manipulations on semiconductors using AFM, we carried out standard lateral atom manipulation experiments. Intrinsic Si adatoms on the Si(111)-(7×7) surface in the presence of a single atomic vacancy were chosen for the lateral atom manipulation experiments [22,38]. The line profiles during atom manipulation,

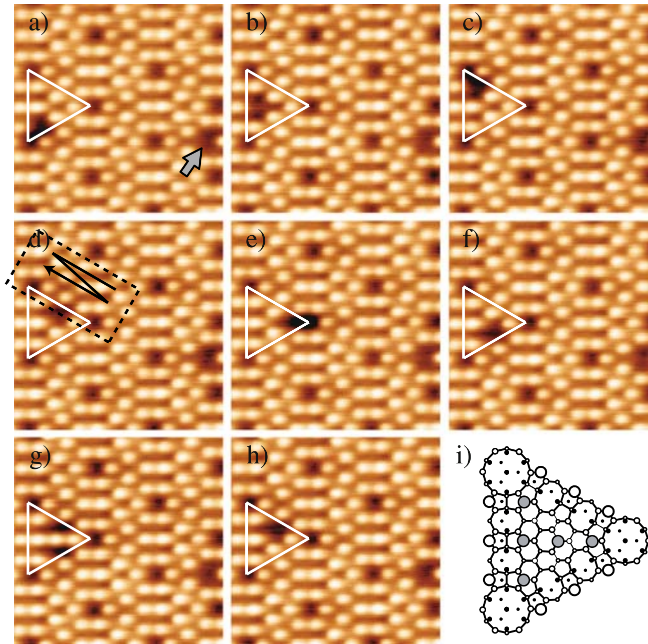

Fig. 8.7. (**a**–**h**) Topographic images selected from a series of vacancy-mediated manipulations of Si adatoms of the Si(111)-(7 × 7) surface. The vacancy indicated by the *gray arrow* in (**a**) is a marker. Image dimensions are 8.0 × 8.0 nm^2. The acquisition parameters are $f_0 = 162{,}295.8$ Hz, $A = 282$ Å, and $k = 28.7$ N m^{-1}. Imaging (Δf_{image}) and manipulation (Δf_{move}) frequency shift set points were −3.9 and −5.1 Hz, corresponding to an attractive chemical bonding force at closest approach of −0.15 and −0.47 nN, respectively. In (**i**), a model of the atomic configuration for the highlighted unit cell in (**g**) is displayed [22]

which include useful information as described further, were analyzed. Furthermore, the chemical bonding force between the AFM tip and the manipulated Si adatom, which was associated with moving the Si adatom, was measured using the same tip as that used for the manipulation.

Figure 8.7a–h shows a selection of AFM images from a series of sequential lateral manipulations of Si adatoms on the Si(111)-(7 × 7) surface. These figures show exactly the same place; the vacancy used as a marker is indicated by the gray arrow in Fig. 8.7a. We manipulated the Si adatoms in a faulted half-unit cell (white triangles) in the presence of an atomic vacancy, which was used as an open space for manipulation at RT. These atomic vacancies can be created [20, 29, 39] or occasionally found. Figure 8.7 shows that the vacancy in the white triangle changes its position, which originates from the manipulation of an Si adatom into the vacancy site. The adatoms adjacent to a vacancy can be individually manipulated along the dimer rows (Fig. 8.7a–f), and across the half-unit cell (Fig. 8.7f–h). The Si adatom can be deposited on

unusual adsorption positions (M sites), as shown in Fig. 8.7g. The model in Fig. 8.7i illustrates the M site, in which the adatom sits in a T_4 configuration bonded to one of the three original surface rest atoms. Si adsorption on this site is stable enough to allow imaging of the Si atom for hours at weak tip–surface interaction forces.

These manipulations have been performed using a similar protocol to the method for interchange lateral atom manipulation described in the previous section. For example, lateral manipulation of an Si adatom from the corner adatom site to the center adatom site, which was performed between Fig. 8.7d and e, is carried out as follows. After obtaining the initial image (Fig. 8.7d), the scan angle is rotated so that the fast scan direction is aligned parallel to the line connecting the vacancy and the Si adatom to be manipulated, and the smaller area indicated by the dotted rectangle is scanned. The tip is scanned near the surface in one direction and lifted 1 Å on the way back to cause directional migration of the atom. Then the slow scan is stopped when the tip scan reaches the line connecting the target adatom and the vacancy. Decreasing the tip–surface distance by changing the setpoint to Δf_{move} induces atom movement. Finally, the initial imaging set point ($\Delta f_{\mathrm{image}}$) is restored, and we obtain the final image shown in Fig. 8.7e. The Si adatom is manipulated in the direction parallel to the fast scan direction.

We found that lateral manipulation strongly depends on the tip asymmetry, as predicted by theoretical calculation [40]. In the series partially shown in Fig. 8.7, the same Δf_{move} set point was used for all the manipulations in the various directions. It is rare to encounter such a highly symmetric tip apex; different Δf_{move} set points are normally required for each manipulation direction. Recent statistical experiments of lateral atom manipulation on the same system using AFM clearly show that the probability of successful atom movements depend dramatically on the scan direction with respect to the tip apex asymmetry, even for crystallographically equivalent directions [38].

The profiles of AFM line scans during manipulation provide information, such as the path of atom hopping and the manipulation mechanism. Figure 8.8c shows the AFM topography during the manipulation carried out between the images in Fig. 8.7d and e. The slow scan is from bottom to top, and the fast scan is from left to right. After imaging the area enclosed by the dotted rectangle in Fig. 8.8c, the slow scan is stopped, and the tip–surface distance is reduced by changing the setpoint to Δf_{move} at the line indicated by the gray arrow. Successive tip scanning on the same line with stronger tip–surface interaction induces atom manipulation. The white arrow indicates the line where the tip–surface distance is restored by changing the setpoint to $\Delta f_{\mathrm{image}}$. Five profiles from successive line scans are displayed in Fig. 8.8b. Profiles B–D obtained with Δf_{move} are sequential, and they correspond to three different stages of the process: before (B), during (C), and after (D) the manipulation. Profiles A and E are topographies with $\Delta f_{\mathrm{image}}$. In profile A, two adatoms are observed at the left corner (Co_{L}) and right corner (Co_{R}) sites and the vacancy is at the center (Ce) site. In profile B, once the left corner

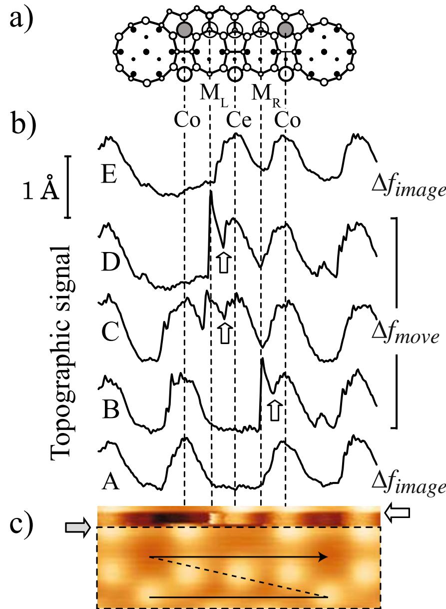

Fig. 8.8. (**a**) Ball-and-stick model of a partial Si(111)-(7 × 7) unit cell with a vacancy on a center (Ce) adatom site. The corner (Co) adatom sites, two equivalent M sites (M_L and M_R), and two H_3 adsorption positions are indicated. (**b**) Line profiles obtained from (**c**), where the topography associated with the manipulation process between the images in Figs. 8.7d, e is displayed. The fast scan velocity was 8.6 nm s^{-1} and the rectangle's dimensions are 4.3 × 1.5 nm^2 [22]

adatom and the vacancy have been imaged, feedback suddenly retracts the tip at the M_R position due to the jump of the right corner adatom toward the tip. The adatom adsorbs on the M_R site until it jumps back to the Co_R site at the tip location marked by the arrow. In profile C, the tip initially encounters and passes over the adatom on the Co_L site and, near the M_L position, it is suddenly retracted due to the jump of the adatom from the Co_L to the M_L site. Subsequently, the adatom jumps again to the Ce site at the tip location marked by the arrow. In profile D, just after the vacancy is imaged, the center adatom jumps toward the tip and adsorbs on the M_L site. Then, it returns to the Ce site at the tip location marked by the arrow. The same atom hopping process as that seen in profile D repeatedly occurs until the Δf_image set point is recovered. This is visualized as the bright feature near the M_L position in Fig. 8.8c. In profile E, the vacancy is finally at the Co_L site, in contrast with profile A.

The comparison of these profiles with previously reported manipulation experiments performed with LT-STM [34,41] indicates that the manipulations reported here can be classified into the so-called pulling mode [34], in which an attractive interaction force with the tip apex pulls the surface adatom

toward the tip position. An Si adatom is manipulated by a local reduction in the natural diffusion barrier that enables thermally activated hopping to adjacent adsorption sites by the attractive chemical bonding force between the tip and the adatom [42,43]. The directionality is imposed by the tip scan direction together with the asymmetric potential energy landscape created by the particular tip–apex structure [38,40]. These ideas are further substantiated with an extensive study by first-principles simulations of the energetics and stability of the Si(111)-(7×7) adatoms in the presence of a vacancy, as well as the modifications induced by the AFM tip. The detailed mechanism of mechanical lateral atom manipulation is discussed in Chap. 11.

An important feature of AFM is the ability to measure the chemical bonding force between the tip apex atoms and surface atoms. The site-specific force spectroscopic technique developed for RT is described in Chap. 2. This capability can be applied to measurements of the chemical bonding force associated with atom manipulation. In Fig. 8.9, a Δf vs. tip–sample distance ($\Delta f - z$) curve on top of the corner adatom is displayed (the dotted curve). This curve was obtained by averaging 80 curves that were repeatedly measured over the same site within a ± 0.1 Å error using an atom tracking technique. The $\Delta f - z$ was converted into the force vs. tip–sample distance ($F - z$) curve by a conversion formula [44]. Then the short-range chemical bonding force displayed in Fig. 8.9 (the solid curve) was obtained by subtracting the long-range force that was estimated from the $F - z$ curve measured over the corner hole. The tip apex state was equivalent in both the force spectroscopy of Fig. 8.9 and atom manipulation of Fig. 8.7. By comparing the $\Delta f - z$ and $F - z$ curves, we can determine the value of the chemical bonding force at the tip–surface distance for both imaging and manipulation. The chemical bonding force exerting the tip just over the adatom during tip scanning with Δf_{image} is estimated to be -0.15 nN. On the other hand, this chemical bonding force becomes -0.47 nN

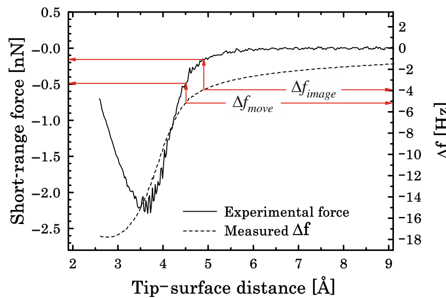

Fig. 8.9. The dotted curve is an averaged $\Delta f - z$ curve resulting from the force spectroscopic measurement on top of the corner adatom using the same tip as that used for the manipulation experiments illustrated in Fig. 8.7. The solid curve is a short-range chemical bonding force converted from the experimental $\Delta f - z$ curve [22]

at the tip–surface distance where an Si adatom can be manipulated during the AFM topographic scan.

8.7 Interchange Vertical Atom Manipulation

We have demonstrated nanostructuring at RT by interchange lateral atom manipulation, as explained in Sect. 8.5. Recently, we have reported a new method for effectively rearranging adatoms on a binary alloy system using interchange vertical atom manipulation. In this method, individual atoms on the tip apex can be deposited on a surface by interchange between a single atom on the tip and a single adatom on the surface. This technique can be regarded as an atomic version of dip-pen nanolithography [45], as one can write patterns on surfaces with atomic precision [19].

The atom manipulation experiments were performed on a Sn/Si(111)-($\sqrt{3} \times \sqrt{3}$) surface. In AFM topographic images of the surface, Sn adatoms and Si adatoms appear as bright and slightly dim spots, respectively, as shown in Fig. 8.10 [26]. Atom manipulation is based on the site-specific force spectroscopic measurement [27,46,47], as described later. First, an AFM image of the surface is acquired, and the target Si adatom is selected for manipulation (the center Si adatom in Fig. 8.10a). Next, the tip is positioned over the topmost part of the Si atom with a lateral precision better than ± 0.1 Å using an atom tracking technique [47]. Then the sample is moved toward the oscillating AFM tip until a jump in the Δf associated with a slight tip modification is observed, as indicated by the arrow in Fig. 8.11a. Scanning the same area as in the previous image after the tip retraction, we find that an Sn atom is deposited on the site that the Si adatom has occupied (Fig. 8.10b). This implies that the Si adatom on the surface has moved to the tip apex; an interchange between the tip apex Sn atom and the surface Si adatom has occurred. The same procedure can then be applied to the opposite process. By moving the tip toward the previously deposited Sn adatom, we can replace the Sn atom by an Si adatom coming from the tip, as shown in Fig. 8.10c. Although the image in Fig. 8.10c shows less contrast than in Fig. 8.10a, b, we can recover good image contrast by scanning a region that neighbors the imaged area at a slightly closer tip–surface distance than that used for imaging (Fig. 8.10d).

Figure 8.11 shows the $\Delta f - z$ curves during (a) the Sn deposition process and (b) the Si deposition process. The black (gray) curve corresponds to approach (retraction). The curves in Fig. 8.11a were obtained during the manipulation process carried out between Fig. 8.10a and b, while those in Fig. 8.11b were obtained between Fig. 8.10b and c. Atom interchanges occurred at the tip–surface distance where the Δf signal jumped, indicated by the arrows in Fig. 8.11. The approach and retraction curves during the Sn deposition process are similar, which implies that the tip apex is not significantly changed (Fig. 8.11a). This is also confirmed by the faint variation of the topographic signal before and after the Sn deposition, as shown in

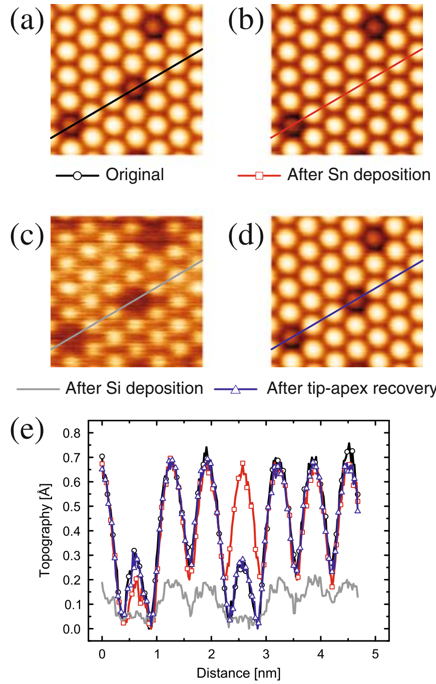

Fig. 8.10. (**a**–**d**) Sequence of AFM images of alternating interchange vertical atom manipulations. (**e**) Line profiles of images of (**a**)–(**d**). Acquisition parameters were $f_0 = 193{,}738.0\,\text{Hz}$, $A = 219\,\text{Å}$, $k = 48.8\,\text{N}\,\text{m}^{-1}$, and a cantilever quality factor (Q) of 13,000. A Δf set point value of $-6.3\,\text{Hz}$ is common to all the topographic images. Experiments were performed at RT [19]

Fig. 8.10e. In contrast, Fig. 8.11b shows that $\Delta f - z$ completely changes after Si deposition: this process considerably modifies the tip apex state. This is also substantiated by the remarkable change in topographic contrast for the image acquired just after Si deposition (Fig. 8.10e). After tip recovery by scanning at slightly closer tip–surface distances, the line profile of Fig. 8.10d is in good agreement with the initial line profile in Fig. 8.10a (Fig. 8.10e). This indicates that the tip apex state can be initialized, and the sequential atom interchange process is completely reversible. The chemical bonding force during atom interchange calculated from the $\Delta f - z$ curves together with the dissipation signals is described in Chap. 3.

Vertical interchange differs from the atom transfer between the STM tip and sample surface previously reported [48]. In previous studies, an atom weakly bonded on a metallic surface was reversibly transferred between the STM tip and the surface by applying a bias voltage. In the present method, a tip apex atom and a surface atom strongly bound to the substrate are interchanged by soft nanoindentation using an AFM tip. Moreover, interchange

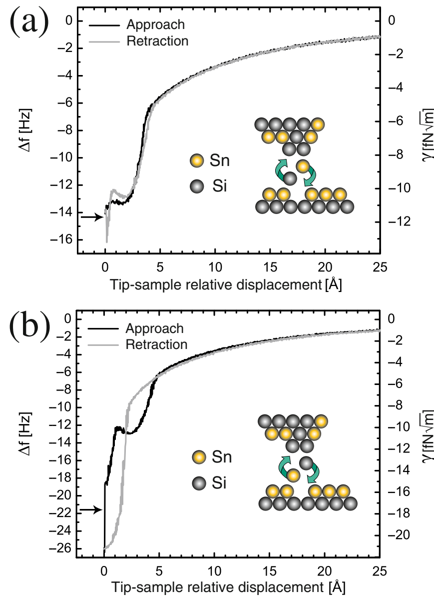

Fig. 8.11. (**a**) Force spectroscopic measurements ($\Delta f - z$ curves) associated with the Sn deposition process shown in Fig. 8.10a, b. (**b**) $\Delta f - z$ curves for the Si deposition shown in Fig. 8.10b, c. The *black* (*gray*) curves correspond to approach (retraction). In the Δf plots, the corresponding normalized frequency shift (γ) is displayed on the right axis [19]

vertical atom manipulation is also different from other mechanical atom manipulation using AFM [18, 22, 49], in which the relatively weak attractive interaction force between tip and sample plays an important role. Vertical atom interchange is induced by a small repulsive interaction force at very close tip–surface distances (see Chap. 3). At such a close distance, a larger contact involving several atoms is expected, leading to a very complex energy landscape. However, the reproducibility of vertical atomic interchange and the resemblance of recorded Δf and force curves in experiments performed with different tips point toward a common basic microscopic mechanism [19]. Details of the manipulation mechanism, including the atomic process, are described in Chap. 11.

From our extensive force spectroscopic measurements on this surface [26, 27], we have found that 29% of the tips can induce atom interchange between tip and surface atoms. Once a tip that produces atom interchange is found, manipulation can be performed in a reproducible way. Moreover, the tips that can produce atom interchange can be classified into three types. The first type can alternately deposit Sn and Si atoms as in Fig. 8.10; the second type can deposit only Sn atoms, and the third can deposit only Si atoms. The tip statistics shows that it is almost equally probable to find tips

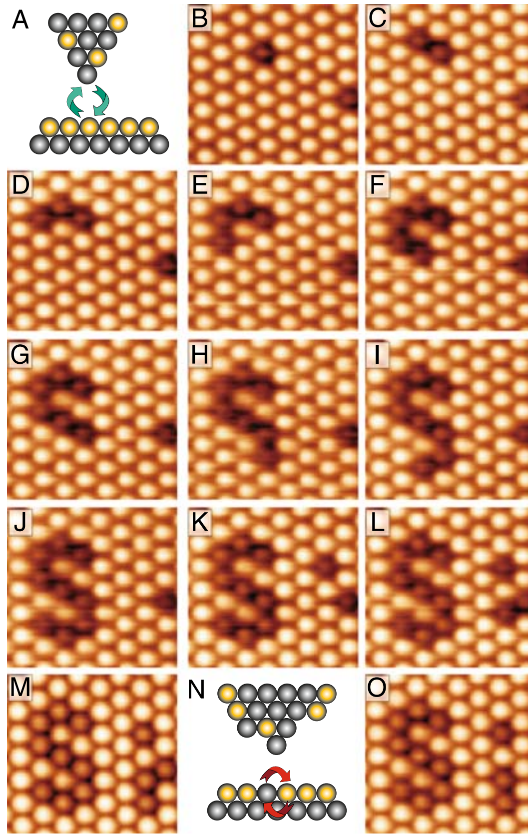

Fig. 8.12. Complex atomic patterning by interchange vertical atom manipulation at RT. (**a**) Illustration of the vertical interchange of atoms between the tip and surface. (**b**–**m**) Series of topographic images showing the creation of atomic patterns displaying the symbol of silicon. These patterns were constructed by the successive deposition of Si atoms coming from the tip onto the Sn monolayer. (**n**) Illustration of the lateral interchange of surface atoms. (**o**) The Si atom adjacent to the "i" character in (**m**) was relocated to a nearby position in several in-plane interchange lateral atom manipulations. Acquisition parameters were $f_0 = 193,744.2$ Hz, $A = 226$ Å, and $k = 48.8\,\mathrm{N\,m^{-1}}$, with imaging Δf set point values between -5.5 and -6.6 Hz

producing either Si deposition or alternate deposition of Sn and Si atoms, and less probable to find one depositing only Sn atoms. By using soft tip–surface contact, we can switch among the three tip types even using the same cantilever, although at present, we have not yet been able to develop a systematic way of producing tips of each type.

To show reproducibility and high precision, we have demonstrated that a nanopattern with atomic precision can be created by interchange vertical atom

manipulation. Figure 8.12 shows the processes of creating the letters "Si" written by Si adatoms embedded on the Sn monolayer. To create these complex atomic patterns, individual Si atoms coming from Si tips were successively deposited on the surface. Since the tip used to create these atomic patterns was type that can only deposit Si atoms, the Si adatom beside the "i" character in Fig. 8.12m was moved away from the character by interchange lateral atom manipulations. Perturbation of the surface structure was not observed during the patterning, as shown in Fig. 8.12. It took 1.5 h to construct the atom letters; the construction time was drastically reduced compared with previous interchange lateral atom manipulation [18].

The study described earlier demonstrated interchange vertical atom manipulation on the Sn/Si(111)-($\sqrt{3} \times \sqrt{3}$) surface. This manipulation method was found to be possible on other semiconductor surfaces as well, such as the In/Si(111)-($\sqrt{3} \times \sqrt{3}$) and Pb/Si(111)-($\sqrt{3} \times \sqrt{3}$) surfaces [19]. Therefore, interchange vertical atom manipulation as well as interchange lateral atom manipulation are expected to be widely used in areas ranging from surface science studies to bottom-up nanotechnology.

8.8 Summary

In this chapter, we reviewed atom manipulation experiments on semiconductor surfaces using AFM. Beginning with vertical and lateral atom manipulation at LT, our group has demonstrated that AFM has the capability of atom manipulation even at RT. Atom manipulation at RT was successfully performed by using intrinsic or substitutional adatoms instead of adsorbates deposited on top of a surface. In particular, the new manipulation methods of interchange lateral/vertical atom manipulation enable us to rearrange adatoms strongly bonded to the substrate with the possibility of patterning complex atomic structures. This new capability of the AFM technique can contribute to the realization of selective semiconductor doping [50], practical implementation of quantum computing [51], or atomic-based spintronics [52]. The possibility of combining sophisticated atom manipulation with the capability of AFM for single-atom chemical identification [27] may bring the advent of future atomic-level applications closer, even at RT.

Acknowledgement

The authors thank their colleagues who contributed to this study: Seizo Morita, Masayuki Abe, Oscar Custance, Noriaki Oyabu.

References

1. D.M. Eigler, E.K. Schweizer, Nature (London) **344**, 524 (1990)
2. J.A. Stroscio, D.M. Eigler, Science **254**, 1319 (1991)
3. M.F. Crommie, C.P. Lutz, D.M. Eigler, Science **262**, 218 (1993)
4. A.J. Heinrich, C.P. Lutz, J.A. Gupta, D.M. Eigler, Science **298**, 1381 (2002)
5. G.V. Nazin, X.H. Qiu, W. Ho, Science **302**, 77 (2003)
6. J.I. Pascual et al., Nature **423**, 525 (2003)
7. N. Nilius, T.M. Wallis, W. Ho, Science **297**, 1853 (2002)
8. T. Komeda et al., Science **295**, 2055 (2002)
9. H.C. Manoharan, C.P. Lutz, D.M. Eigler, Nature **403**, 512 (2000)
10. S.-W. Hla, L. Bartels, G. Meyer, K.H. Rieder, Phys. Rev. Lett. **85**, 2777 (2000)
11. B.C. Stipe, M.A. Rezaei, W. Ho, Science **279**, 1907 (1998)
12. B.C. Stipe, M.A. Rezaei, W. Ho, Phys. Rev. Lett. **78**, 4410 (1997)
13. G. Meyer, S. Zophel, K.H. Rieder, Phys. Rev. Lett. **77**, 2113 (1996)
14. H. Uchida, D. Huang, F. Grey, M. Aono, Phys. Rev. Lett. **70**, 2040 (1993)
15. F.J. Giessibl, Science **267**, 68 (1995)
16. S. Kitamura, M. Iwatsuki, Jpn. J. Appl. Phys. **34**, 145 (1995)
17. S. Morita, R. Wiesendanger, E. Meyer (eds.), *Noncontact Atomic Force Microscopy* (Springer-Verlag, Berlin Heidelberg New York, 2002)
18. Y. Sugimoto et al., Nat. Mater. **4**, 156 (2005)
19. Y. Sugimoto et al., Science **322**, 413 (2008)
20. N. Oyabu et al., Phys. Rev. Lett. **90**, 176102 (2003)
21. N. Oyabu et al., Nanotechnology **16**, S112 (2005)
22. Y. Sugimoto et al., Phys. Rev. Lett. **98**, 106104 (2007)
23. N. Suehira, Y. Tomiyoshi, Y. Sugawara, S. Morita, Rev. Sci. Instrum. **72**, 2971 (2001)
24. F.J. Giessibl et al., Nanotechnology **15**, S79 (2004)
25. I. Horcas et al., Rev. Sci. Instrum. **78**, 013705 (2007)
26. Y. Sugimoto et al., Phys. Rev. B **73**, 205329 (2006)
27. Y. Sugimoto et al., Nature (London) **446**, 64 (2007)
28. M. Abe, Y. Sugimoto, S. Morita, Nanotechnology **16**, S68 (2005)
29. S. Morita et al., Appl. Surf. Sci. **241**, 2 (2005)
30. I.W. Lyo, P. Avouris, Science **253**, 173 (1991)
31. I.W. Lyo, P. Avouris, Science **259**, 1724 (1993)
32. Y. Sugawara, Y. Sano, N. Suehira, S. Morita, Appl. Surf. Sci. **188**, 285 (2002)
33. B.C. Stipe, M.A. Rezaei, W. Ho, Phys. Rev. Lett. **79**, 4397 (1997)
34. L. Bartels, G. Meyer, K.-H. Rieder, Phys. Rev. Lett. **79**, 697 (1997)
35. E. Ganz, S.K. Theiss, I.S. Hwang, J. Golovchenko, Phys. Rev. Lett. **68**, 1567 (1992)
36. I.S. Hwang, J. Golovchenko, Science **258**, 1119 (1992)
37. Y. Sugimoto, O. Custance, M. Abe, S. Morita, e-J. Surf. Sci. Nanotech. **4**, 376 (2006)
38. Y. Sugimoto, K. Miki, M. Abe, S. Morita, Phys. Rev. B **78**, 205305 (2008)
39. S. Kawai H. Kawakatsu, Appl. Phys. Lett. **89**, 023113 (2006)
40. L. Pizzagalli, A. Baratoff, Phys. Rev. B **68**, 115427 (2003)
41. S.W. Hla, K.F. Braun, K.H. Rieder, Phys. Rev. B **67**, 201402 (2003)
42. G. Meyer et al., Phys. Rev. Lett. **78**, 1512 (1997)
43. M.B. Watkins, A.L. Shluger, Phys. Rev. B **73**, 245435 (2006)

44. J.E. Sader, S.P. Jarvis, Appl. Phys. Lett. **84**, 1801 (2004)
45. R. Piner et al., Science **283**, 661 (1999)
46. M.A. Lantz et al., Science **291**, 2580 (2001)
47. M. Abe, Y. Sugimoto, O. Custance, S. Morita, Appl. Phys. Lett. **87**, 173503 (2005)
48. D.M. Eigler, C.P. Lutz, W.E. Rudge, Nature (London) **352**, 600 (1991)
49. M. Ternes et al., Science **319**, 1066 (2008)
50. T. Shinada, S. Okamoto, T. Kobayashi, I. Ohdomari, Nature **437**, 1128 (2005)
51. B. Kane, Nature **393**, 133 (1998)
52. D. Kitchen et al., Nature **442**, 436 (2006)